Archives of Advances in Biosciences

Original Article

OPEN ACCESS

Simultaneous Inhibition of Histone Deacetylases and EZH2 Reduces SASP in Non-Small Cell Lung Cancer

Hak-Song Kim[1, 4], Sun-Hyok Kong[1, 4], Chol Jin Pak [1, 3, 4*], Jong-Chol Jang[1], Bong-Su Ri[1], Kum-Chol Ri[1], Kum-Chol Kim[1], Yong-Min Ri[1], Chol-Ho Ju[1], Gyong Min Hwang [1], Un Song Ri[2]

[1.] School of Life Science, University of Science, Pyongyang, Democratic People's Republic of Korea.
[2.] College of Life Science, **Kim Il Sung** University, Pyongyang, Democratic People's Republic of Korea.
[3.] College of Life Science, Northeast Agricultural University, Harbin, China. Email:15504506210@163.com
[4.] These authors contributed equally: Hak-Song Kim, Sun-Hyok Kong, Chol Jin Pak.

Received: 16 Dec, 2025; **Accepted:** 06 Jan 2026; **Published:** 11 Jan 2026

Cite this article as: Kim H-S, Kong S-H, Pak C-J, Jang J-C, Ri B-S, Ri K-C, et al. Simultaneous Inhibition of Histone Deacetylases and EZH2 Reduces SASP in Non-Small Cell Lung Cancer. Archives of Advances in Biosciences. 2025 16(1):1-10. https://doi.org/10.22037/aab.v16i1.51195

Abstract

Background and Aim: Cellular senescence, a common outcome of treatments like chemotherapy and radiotherapy, often acts as a therapeutic hurdle. Our prior investigations revealed that this senescent state is accompanied by the secretion of the senescence-associated secretory phenotype (SASP), a potent driver of chronic inflammation and a factor that can paradoxically facilitate tumor progression.

Methods: We investigated the effects of SAHA, alone or combined with the EZH2 inhibitor EPZ-6438, on NSCLC cell lines. Senescence induction was confirmed via SA-β-galactosidase staining, while cell growth was evaluated using MTT and colony formation assays. Mechanistic studies, including Western blotting, qPCR for SASP factors, and immunofluorescence for Cytoplasmic Chromatin Fragments (CCF), were performed to assess the underlying pathway.

Results: SAHA effectively induced senescence-mediated growth inhibition in A549 and H1299 cells but simultaneously triggered the SASP. This SAHA-induced SASP was linked to the generation of CCFs, thereby activating the cGAS–STING pathway. Importantly, the combined administration of SAHA and EPZ-6438 significantly reduced the expression of inflammatory mediators, such as IL6 and IL8. This co-treatment not only provided superior anti-proliferative activity compared to SAHA alone but also enhanced the suppression by attenuating the SASP.

Conclusion: Collectively, our data demonstrate that SAHA-induced senescence in NSCLC cells is critically linked to detrimental SASP production mediated by CCF formation. Crucially, combining SAHA with EZH2 inhibition successfully suppressed the SASP, leading to enhanced growth inhibition, thereby providing a robust rationale for this combination therapy in NSCLC treatment.

Keywords: Non-small cell lung cancer (NSCLC); Suberoylanilide Hydroxamic Acid (SAHA); Enhancer of zeste homolog 2(EZH2); senescence; senescence-associated secretory phenotype (SASP)

1. Introduction

Lung cancer remains the principal cause of cancer-related mortality globally (1). Non-small cell lung cancer (NSCLC), encompassing squamous cell carcinoma, adenocarcinoma, and large-cell carcinoma, constitutes the majority of clinical cases (2) Despite substantial progress in therapeutic modalities, a poor overall prognosis persists, largely due to the frequent occurrence of disease recurrence and therapy resistance(3).

Cellular senescence, characterized by an irreversible proliferative arrest, primarily functions as an innate defense against cancer development (4, 5). Intriguingly, accumulating data reveal a complex duality, where chemotherapy-triggered senescence can sometimes promote tumor relapse(4, 5). A key aspect of this paradoxical role is the Senescence-Associated Secretory Phenotype (SASP) (6, 7) This heterogeneous cocktail of signaling molecules, including pro-inflammatory cytokines, chemokines, and growth factors (8-10), initially helps clear pre-malignant cells. However, when SASP is sustained or unregulated, it establishes a chronic, pro-tumorigenic microenvironment that promotes angiogenesis, epithelial-mesenchymal transition (EMT), and proliferation (11-13) The challenge now lies in optimizing cancer therapy to retain the benefits of growth arrest while neutralizing the harmful effects of SASP(14).

The precise mechanism governing SASP induction involves the formation of cytoplasmic chromatin fragments (CCFs)—nuclear DNA debris mislocalized to the cytosol (15-17). These fragments are recognized by the innate immune sensor cGAS (cyclic GMP–AMP synthase), which, in turn, leads to the activation of STING (stimulator of interferon genes), initiates an inflammatory cascade central to SASP factor transcription (15, 17, 18). This connection links genomic instability directly to pro-tumorigenic signaling.

Histone deacetylases (HDACs) are pivotal regulators of chromatin structure, functioning through the removal of acetyl groups from histone lysine residues (19). Dysregulated HDAC activity is a common feature across multiple malignancies, positioning these enzymes as attractive therapeutic targets (20, 21). Among the developed anticancer agents, the HDAC inhibitor Vorinostat (SAHA) is recognized for its ability to induce senescence in various cancer cell types (4,22,23). Furthermore, our group has previously established a role for enhancer of zeste homolog 2 (EZH2), a major H3K27 methyltransferase, in promoting both CCF formation and cGAS–STING pathway activation, contributing to SASP in both breast and small-cell lung cancer (SCLC) models (24, 25)

Building upon this mechanistic insight, we hypothesized that the detrimental SASP phenotype observed in NSCLC—a distinct and clinically challenging entity could be effectively attenuated by combining the HDAC inhibitor SAHA with the EZH2 inhibitor EPZ-6438. Here, we rigorously demonstrate that while SAHA induces senescence and the concurrent SASP in A549 and H1299 NSCLC cells, the addition of EPZ-6438 selectively suppresses SASP output, significantly boosting SAHA's anti-proliferative efficacy. These data propose a novel strategy for improving NSCLC therapy by specifically targeting the pro-tumorigenic SASP component of senescence.

2. Methods

Cell culture

The human NSCLC cell lines NCI-A549 and NCI-H1299 were sourced from the American Type Culture Collection (ATCC). Cells were maintained at 37°C in a humidified 5% CO_2 atmosphere. The culture medium used was DMEM supplemented with 10% fetal bovine serum (FBS) and a standard cocktail of antibiotics (100 U/mL penicillin, 100 µg/mL streptomycin). Frozen stocks were used to establish fresh cultures at two-month intervals to ensure experimental integrity. Mycoplasma contamination was routinely assessed at two-month intervals using a Mycoplasma Test kit (LT07-218, Lonza, Basel, Switzerland)

SA-β-galactosidase staining

The SA-β-galactosidase staining buffer (pH 6.0) was freshly prepared using 20× KC [1.64g K3Fe(CN)6, 2.1g K4Fe(CN)6 3H2O in 50mL PBS] and 20× X-gal [40mg/ml X-gal in N, N-dimethylformamide], diluted into PBS containing 1mM $MgCl_2$. Cells were fixed for 15 minutes at room temperature using 0.5% glutaraldehyde in PBS (pH 7.4). Following fixation and two washes with PBS/$MgCl_2$ (pH 6.0), the prepared staining solution was administered. Incubation was performed in the dark at 37 °C for 14–16 h.

Immunofluorescence

Cells were washed twice with PBS, 4% paraformaldehyde solution was added to the cells, and the cells were subsequently fixed for 10 min and rinsed twice with PBS. Cells were permeabilized with 0.5% Triton X-100 solution (0.5% Triton X-100 in PBS) for 10 min and washed twice with PBS. Then, using the TBST solution containing 5% BSA was blocked up cells for 1 h. Cells were incubated at 4°C with primary antibody for overnight. And cells were washed three times for 5 min with TBST solution, and the secondary antibody was added and incubated for 1 h at 37 °C. Cells were washed three times for 5 min in TBST solution again, and then nuclei were stained with 500 nM DAPI for 10 min and observed using a confocal microscope (OLYMPUS). The antibodies used in the experiments were as follows: Anti-H3K27me3 (Activemotif, 39535), Anti-γH2AX (Cell Signaling Technology, 9718S), Anti-γH2AX (Cell Signaling Technology, 80312S), Goat anti-Rabbit IgG (H+L) Cross-Adsorbed Secondary Antibody (Alexa Fluor™ 488 (Invitrogen A11008)), Goat anti-Mouse IgG (H+L) Highly Cross-Adsorbed Secondary Antibody

(Alexa Fluor™ 488 (Invitrogen A11029))

CCF assay and quantitative analysis

CCFs were detected via immunofluorescence using antibodies targeting the DNA damage marker γH2AX and the repressive chromatin marker H3K27me3. Following DAPI counterstaining, CCFs were strictly identified as DAPI-positive foci that co-localized with both γH2AX and H3K27me3 signals, located distinctly outside the main nucleus. The frequency of CCF-positive cells was determined by counting a minimum of 100 random cells per condition, with all counting performed independently by two blinded investigators.

Preparation of Conditional Medium (CM)

A549 and H1299 cells were seeded at 5×10^6 cells per 10 cm plate. After a 48-hour incubation with the respective treatments (DMSO, 2 μM SAHA, or 2 μM SAHA + 0.5 μM EPZ-6438), the culture medium was removed by aspiration.Cells were gently washed with PBS and then supplemented with 10 ml of fresh, drug-free DMEM containing 10% FBS. Following an additional 24-hour incubation to allow factor secretion, the conditioned medium (CM) was collected. Cell debris was removed by centrifugation (1,500 rpm for 5 min), and the medium was sterilized using a 0.2 μm filter before use in subsequent experiments.

Measurement of cell proliferation rate

Cell proliferation was quantitatively evaluated using the conventional MTT assay. NSCLC cells were plated into 96-well microplates at a density of 2,000 cells per well. The cells were then exposed to the experimental compounds (SAHA and EPZ-6438) in DMEM containing 10% FBS for a total period of 72 hours. Vehicle-treated cells (DMSO) were concurrently run as the negative control group. Cell viability was monitored at 24-hour intervals. To facilitate this assessment, 20 μL of the MTT solution (prepared at a concentration of 5 mg/mL in PBS) was introduced to each well, and the plates were allowed to incubate for four hours at 37 °C. Subsequently, the culture media was carefully removed, and 100 μL of DMSO was added to fully solubilize the formazan crystals that had formed. After a brief 10-minute agitation step, the optical density was quantified spectrophotometrically at a wavelength of 492 nm.

Colony formation analysis

For the colony formation assay, NSCLC cells were inoculated into 6-well culture plates at a density of 9,000 cells per well. Cells were initially exposed to SAHA and EPZ-6438 (in DMEM supplemented with 10% FBS) over a continuous 72-hour period. After this phase, the treatment medium was fully aspirated and replaced with either fresh, untreated DMEM or the corresponding conditioned medium (CM). Cultures were maintained for a total of 15 days, with a complete medium refresh performed every three days. The final colony formation efficiency was determined by quantifying the percentage of initial plated cells that successfully developed into observable colonies.

Western blotting

For protein analysis, cells were collected after a PBS wash and lysed using 1×Laemmli sample buffer. The resulting lysates were separated by SDS-PAGE, followed by transfer to PVDF membranes. The following antibodies were used: Anti-IL6 (Immunoway, YT5348), Anti-STING (Abways, CY7204), Anti-p-STING (Cell Signaling Technology, 19781), Anti-EZH2 (Abways, Q15910), Anti-Cyclin A2 (Cell Signaling Technology, 67955S), Anti-H3K27me3 (Activemotif, 39535), Anti-β-actin (Sigma-Aldrich, A1978), Anti-p21 (Proteintech, 10355-1-AP), Anti-Histone H3 (abcam, ab1791), Anti-acetyl-Histone H3 (Millipore, 06-599), and secondary goat anti-mouse and goat anti-rabbit antibodies (ZSGB-BIO; Beijing, China).

Reverse transcription, PCR, and quantitative real-time PCR(qPCR) analysis

Total RNA extraction, reverse transcription, and quantitative PCR (qPCR) were conducted generally following our established methods (25). Total RNA was isolated from cells using the RNAiso Plus kit. Reverse transcription was carried out using a commercial Reverse Transcription System to synthesize cDNA. Target gene quantification was performed on the cDNA using a 2× Taq Master Mix kit. Relative gene expression was calculated using the $2^{-\Delta\Delta Ct}$ method, normalized to the internal control β-actin mRNA. The primers utilized for qPCR analysis are listed below: β-actin; sense 5'-GAGCACA-GAGCCTCGCCTTT-3', β-actin antisense 5'-ATCCTTCTGACCCATGCCCA-3', IL-6 sense 5'-CCCCTGACCCAACCACAAAT-3', IL-6 antisense 5'-ATTTGCCG-AAGAGCCCTCAG-3', IL-8 sense 5'-GAGTGGACCACACTGCGCCA-3', IL-8 antisense 5'-TCCACAACCCTCTGC-ACCCAGT-3'

Statistical analysis

All data were presented the results of at least three independent experiments and delineated as mean ± SD. Data were considered statistically significant at $P < 0.05$. Statistical analysis was performed using Prism 8 (GraphPad Software).

3. Results

Inhibition of HDAC induces senescence in NSCLC

cells

To investigate the effect of the HDAC inhibitor SAHA on NSCLC cells, we treated A549 and H1299 lines with various SAHA concentrations to identify a senescence-inducing dose. We found that 2 µM SAHA effectively decreased the expression level of the proliferation marker Cyclin A2 while significantly upregulating the senescence-associated marker p21 (Fig. 1A and 1B). This suggested that SAHA promotes histone acetylation and senescence in A549 and H1299 cells. Time-course analysis using H1299 cells confirmed that these changes in Cyclin A2 and p21 expression became significant from 60 hours onward (Fig. 1C). Furthermore, SAHA treatment significantly increased senescence-related β-galactosidase activity in both cell lines (Fig. 1D, 1E, 1F). These findings confirm that SAHA inhibits NSCLC cell growth by inducing senescence.

HDAC inhibition produces SASP in NSCLC cells

Given that SASP acts as both a marker of senescence (7) and a promoter of tumor progression (13), we next assessed whether SAHA also induced SASP in NSCLC cells. We focused on IL6, a major SASP factor. Western blot analysis showed an increase in IL6 protein following SAHA exposure, which was prominent in A549 cells and observable in H1299 cells (Fig 2A and 2B). Quantitative PCR (qPCR) further confirmed a significant transcriptional upregulation of the key SASP factors IL6 and IL8 in both cell lines after SAHA treatment (Fig 2C and 2D). Therefore, SAHA induces not only senescence but also concomitant SASP secretion in NSCLC cells.

HDAC inhibition induces CCF in NSCLC cells to produce SASP

CCF production has been linked to SASP induction triggered by DNA damage and oncogene activation in previous reports (15). SAHA treatment has also been reported to induce senescence and CCF simultaneously in SCLC cells (29). We first confirmed DNA damage response using immunofluorescence for γH2AX, which showed increased expression in both SAHA-treated A549 and H1299 cells (Fig 3A and 3B). CCFs are characterized by positivity for DAPI, γH2AX, and H3K27me3 (15). Measuring these markers, we observed a significant increase in triple-positive CCFs in SAHA-treated NSCLC cells (Fig 3C-3F). Since CCFs are recognized by cGAS, leading to STING-mediated SASP production (15, 17), we assessed the cGAS-STING pathway. SAHA treatment increased p-STING expression, and co-treatment with the STING inhibitor CCCP (29) suppressed both p-STING and IL6 expression (Fig 3G and 3H). These results indicate that SAHA-induced SASP in NSCLC cells is mediated by CCF generation and subsequent activation of the cGAS–STING pathway.

EZH2 Inhibitor EPZ-6438 inhibits SASP induced by SAHA in NSCLC cells

Previous work from our group and others has established a mechanistic link between EZH2 activity, the generation of cytoplasmic chromatin fragments (CCF), and the subsequent secretion of the pro-tumorigenic SASP in both small cell lung cancer (SCLC) (25, 26) and breast cancer models (where it also drives metastasis) (24). Given that EZH2 is a methyltransferase responsible for H3K27 trimethylation and is frequently overexpressed in lung malignancies (27), we proceeded to investigate its therapeutic relevance in NSCLC.

We initially performed a dose–response analysis to determine the optimal working concentration of the specific EZH2 inhibitor, EPZ-6438, when used in conjunction with SAHA (Fig 4A and 4B). By assessing the resultant H3K27me3 protein levels—a direct measure of EZH2 enzymatic activity—we found that effective inhibition was achieved even at the lowest concentration tested (0.1 µM EPZ-6438 with SAHA). However, to ensure maximal and sustained pharmacological blockade for the subsequent functional assays, a robust concentration of 0.5 µM EPZ-6438 was selected for all combination treatments.

The combined SAHA/EPZ-6438 regimen resulted in a substantial reduction in the protein expression of the SASP factor IL-6 when compared to SAHA alone. Importantly, the suppression of SASP was achieved without compromising the core senescence phenotype, as indicated by the stable expression levels of Cyclin A2 and p21, which were comparable to the SAHA single treatment group (Fig 4C and 4D). This SASP attenuation was further corroborated at the transcriptional level, showing a significant decrease in the mRNA abundance of both IL-6 and IL-8 following the dual inhibition (Figures 4E and 4F).

Inhibition of SASP inhibits the proliferation in NSCLC cells

We initiated an assessment of the anti-proliferative efficacy delivered by the combined SAHA and EPZ-6438 regimen in NSCLC cell lines. MTT assays clearly demonstrated that this co-treatment provided a significantly stronger suppression of cell proliferation compared to SAHA monotherapy (Fig 5A and 5B). Complementing this, the colony formation assay revealed that the combination therapy yielded a markedly lower survival rate for treated cells than SAHA administered alone (Fig 5C). To functionally validate the role of the SASP secretome in promoting NSCLC growth, we conducted subsequent colony formation experiments utilizing conditioned medium

Archives of Advances in Biosciences

(CM) derived from the treated cells (Fig 5D). The results showed that the presence of SASP factors enhanced cancer cell growth, whereas their absence significantly inhibited it (Fig 5F). This indicates that the EPZ-6438 and SAHA co-treatment not only inhibits cancer cell proliferation directly but also does so indirectly by attenuating SASP.

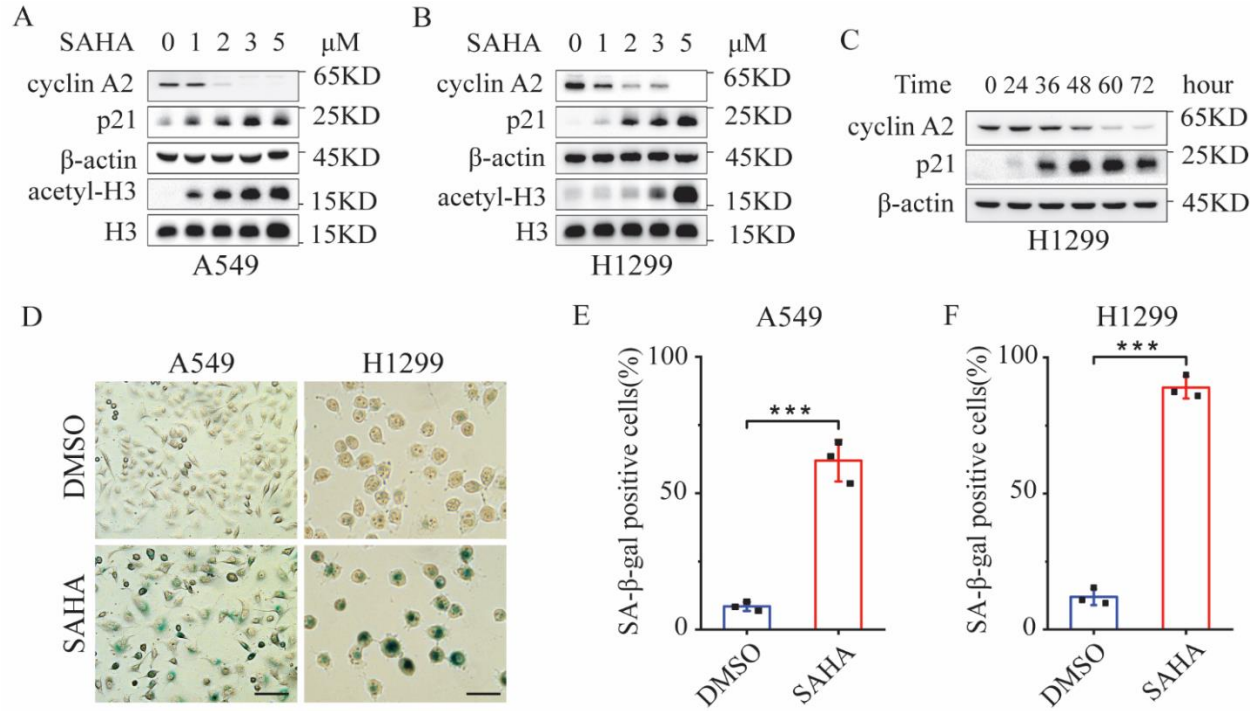

Figure 1. HDAC inhibition induces senescence in NSCLC cells. A, B: The senescence-related proteins and histone acetylation in A549(A) and H1299(B) cells treated with different concentrations of SAHA for 3 days, assessed using western blotting. C: After treatment of H1299 cells with 2μM SAHA, the expression levels of senescence-related proteins with treatment time assessed using western blotting. D: Figure shows the senescence-related β-galactosidase activity of A549 and H1299 cells after treatment with 2μM SAHA for 3 days. Scale bar = 50μm. E, F: A549(E) and H1299(F) cells treated with SAHA showed a positive percentage of senescence-related β-galactosidase activity among more than 100 cells. The replication of individual experiments was three times, * * * P<0.001.

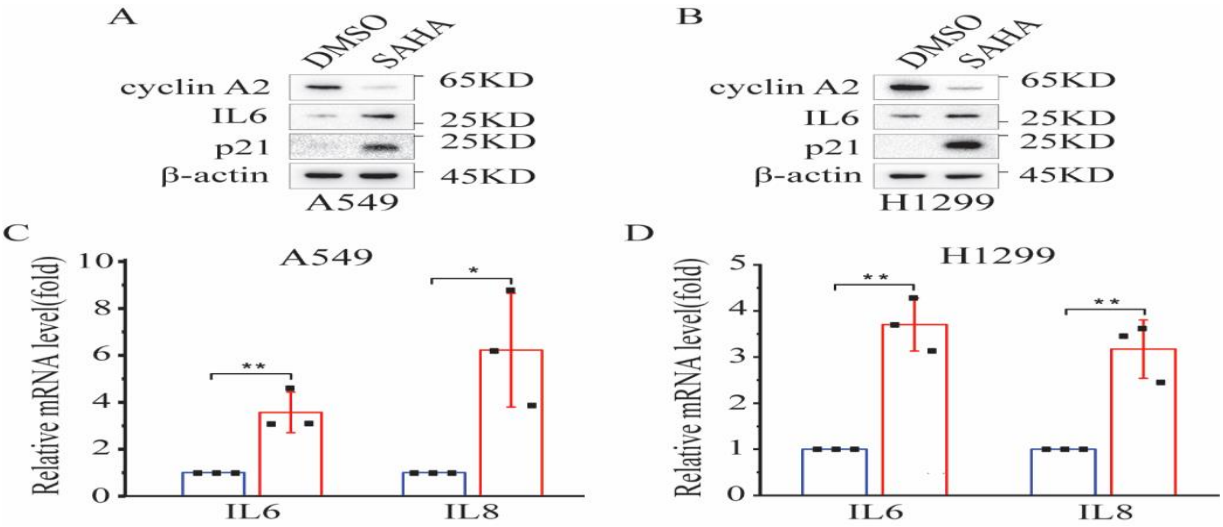

Figure 2. HDAC inhibition is accompanied by SASP with senescence in NSCLC cells. A, B: After treatment of A549 (A) and H1299 (B) cells with 2μM SAHA for 3 days, the protein levels of IL6 were assayed using Western blotting. C, D: RT-PCR assessed

mRNA levels of IL6 and IL8 in A549 (C) and H1299 (D) cells treated with 2μM SAHA for 3 days. The number of replication = 3, mRNA levels were quantified by comparison with the level of β-actin mRNA. * P<0.05, * * P<0.01 compared with the corresponding control.

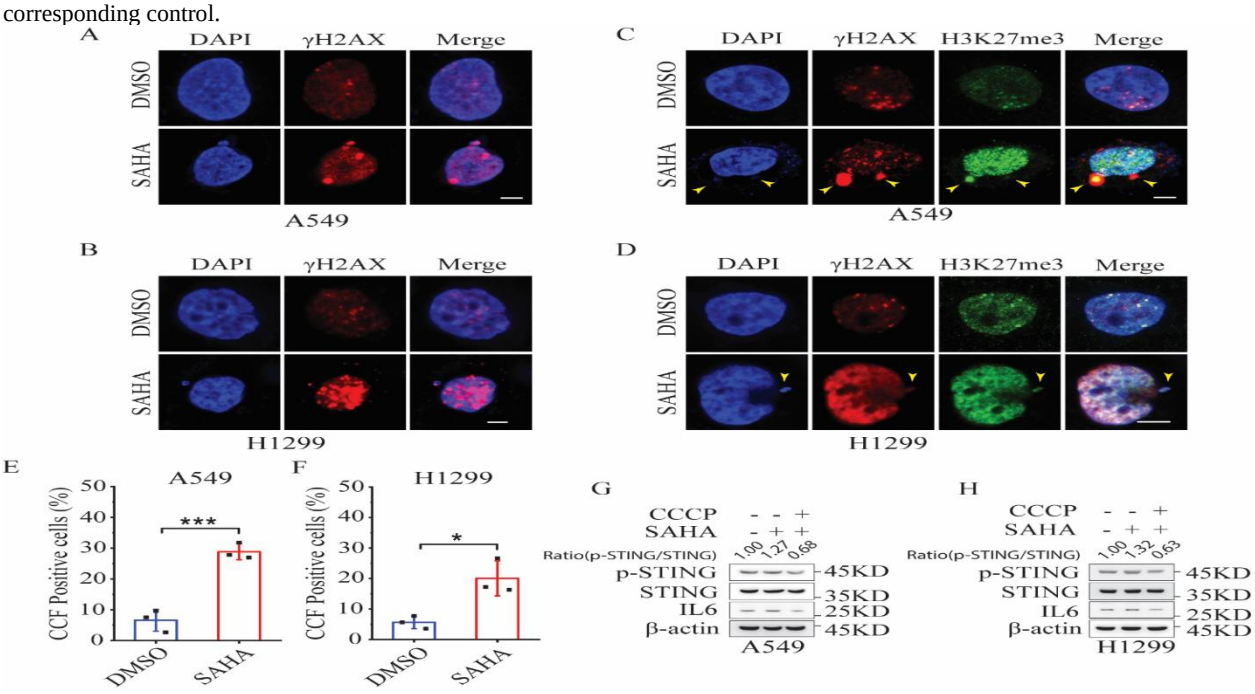

Figure 3. The production of CCF by HDAC inhibition in NSCLC cells is associated with SASP. A, B: Using immunofluorescence images with γH2AX antibodies, assessed DNA damage responses in A549 (A) and H1299 (B) cells. Scale bar = 10μm, C, D: Using γH2AX antibody and H3K27me3 antibody, assessed the development of CCF after SAHA treatment in A549(C) and H1299(D) cells. Scale bar = 10μm, E, F: The incidence of CCF was evaluated by monitoring 100 cells after DMSO and SAHA treatment in A549(E) and H1299(F) cells. Error bars indicate Mean ± SD, n = 3, * P<0.05 and * * * P<0.001, compared with the control. G, H: Western blotting evaluated the expression levels of cGAS-STING pathway-associated proteins in A549 (G) and H1299 (H) cells treated with 2μM SAHA and 10μM CCCP (STING inhibitor), SAHA was treated for 3 days and CCCP was treated for 24 h.

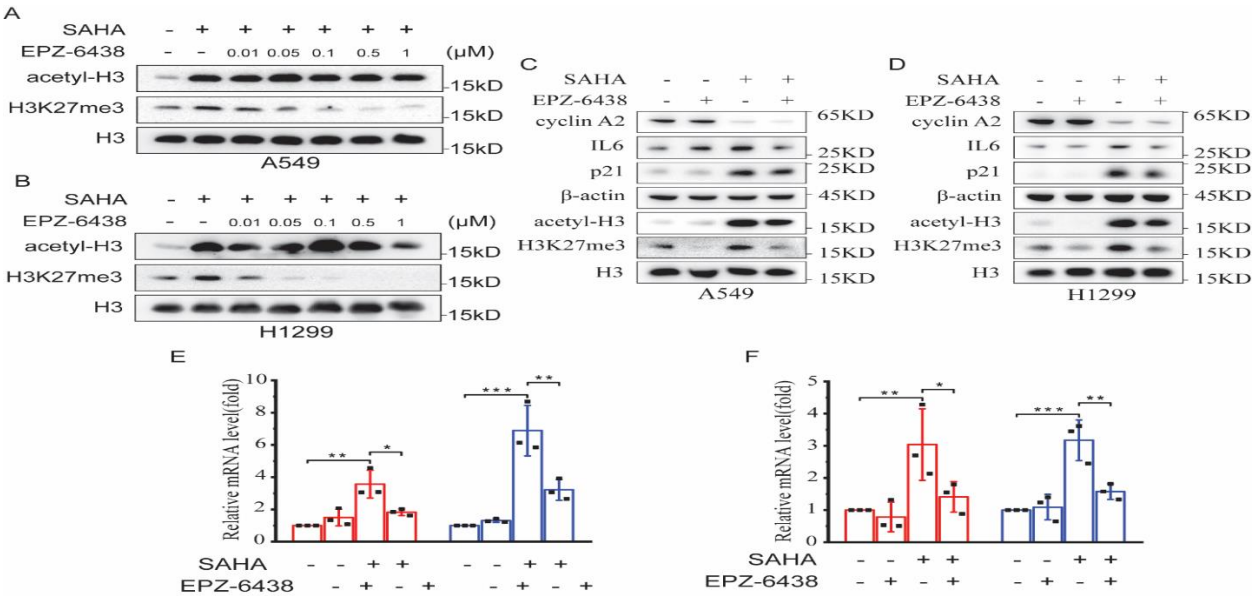

Figure 4. The inhibition of HDAC and EZH2 inhibited SASP in NSCLC cells. A, B: A549 (A) and H1299 (B) cells were treated with 2μM SAHA and different concentrations of EPZ-6438 and analyzed after 3 days. H3 was used as a control. C, D: After 3 days of treatment with 2μM SAHA and 0.5μM EPZ-6438, the expression levels of senescence-related proteins and IL6 proteins were

used to evaluate using western blotting in A549(C) and H1299(D) cells. E, F: Treatment of A549(E) and H1299(F) cells was performed as above and mRNA levels of IL6 and IL8 were examined using RT-PCR. mRNA levels were quantified by comparison with the levels of β-actin mRNA, * P<0.05, * * P<0.01, * * * P<0.001 were marked as compared to the control.

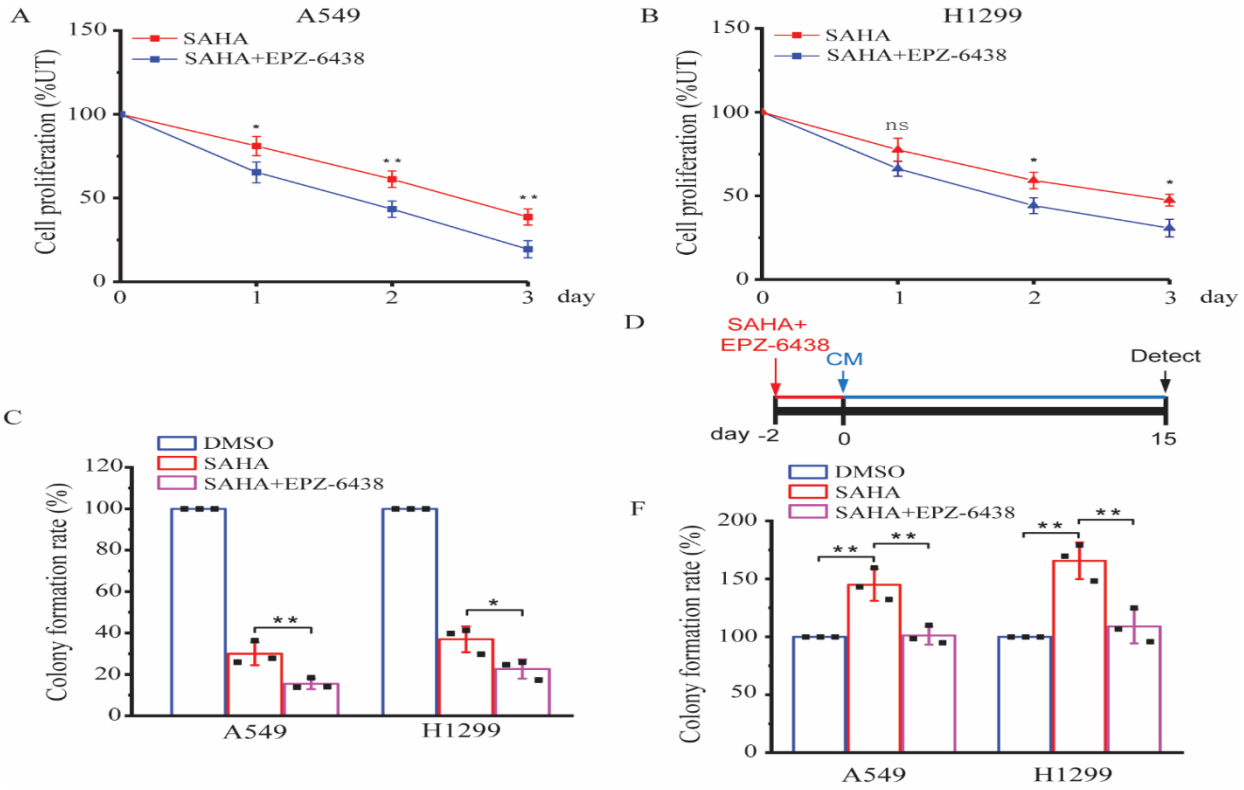

Figure 5. The antiproliferative effect of SAHA in NSCLC cells is enhanced by inhibition of SASP. A, B: Using the MTT assays, the proliferation rate of cells was evaluated at 1-day intervals in A549 (A) and H1299 (B) cells co-treated with 2μM SAHA or 2μM SAHA and 0.5μM EPZ-6438. The value of each treatment was estimated as the percentage of proliferation compared to the control group using the untreated (UT) group as a control. C: A549 and H1299 cells were treated with DMSO, 2μM SAHA or 2μM SAHA and 0.5μM EPZ-6438 for 3 days, and after 15 days the percentage of colony formation was shown compared to DMSO treatment. Each experiment was expressed as Mean ± SD of three independent experiments. D: Scheme shows the experimental design to evaluate the activity of SASP after co-treatment of 2μM SAHA and 0.5μM EPZ-6438 in NSCLC cells in E. E: After co-treatment with 2μM SAHA and 0.5μM EPZ-6438 cells, the colony formation rate was evaluated after 15 days of incubation on prepared CM medium. Each experiment was repeated three times and the experimental values are expressed as Mean ± SD. ns: No significant level of significance compared to the control, * P<0.05, * * P<0.01, * * * P<0.001 were marked as compared to the control.

4. Discussion

In this study, we demonstrated that therapeutic administration of the HDAC inhibitor SAHA in NSCLC models provokes a dual response: the advantageous induction of cellular senescence concomitant with the deleterious secretion of SASP factors. Mechanistically, we found that this pro-tumorigenic secretome originates from the accumulation of cytosolic DNA fragments (CCFs), which subsequently engage the cGAS-STING innate immune signaling cascade. Critically, the addition of the EZH2 inhibitor, EPZ-6438, serves to selectively uncouple these processes by effectively dampening SASP secretion. This mitigation of the secretome, in turn, significantly amplifies SAHA's intrinsic growth-inhibitory effects on the lung cancer cells, providing vital context for managing the complex, often contradictory roles that cellular senescence plays in the anti-cancer response. In particular, the occurrence of senescence in tumors has been considered as an effective anticancer therapy because of its inhibitory effect against cancer development and progression (27). Cells generally experience the senescence as a response to DNA damage, oxidative stress, telomere shortening, and oncogene stimulation (16). Anticancer drugs have been reported to induce cancer cell senescence during treatment, particularly SAHA, in various cancer cell types (4). Consistent with existing literature, our results confirm SAHA's ability to drive

senescence in both the A549 and H1299 cell lines. Yet, the effective drug concentration and required treatment duration for NSCLC were found to be different from those reported in studies focusing on small-cell lung cancer (SCLC), underscoring the intrinsic cell type-dependency of the senescence response to SAHA. Mechanistically, senescence induced by chemotherapeutic agents targeting DNA is known to generate a significant DNA Damage Response (DDR), often culminating in double- or single -strand breaks (29). When this DNA damage occurs, the resulting fragments are often found in the cytoplasm, forming foci that co-localize with the cGAS sensor and the damage marker γH2AX (16). This recognition of cytosolic DNA is the essential trigger that links the damaged chromatin to the cGAS–STING signaling pathway, which then culminates in the secretory phenotype (SASP) (15). The induction of the SASP in senescent cells has been established by our group and others as a process mechanistically driven by the cGAS–STING pathway, which is triggered by the translocation of chromatin material into the cytoplasm (CCF) (15, 16, 25). Our data confirmed that SAHA treatment concurrently induces DNA damage repair activation and facilitates CCF formation in NSCLC cells. To functionally validate the cGAS–STING axis in this response, we employed CCCP, an agent documented to suppress STING activation and the subsequent production of Type I IFNs (30). Upon examining the IL-6 expression levels induced by SAHA in the presence of CCCP, we noted a significant reduction compared to the SAHA-only group. This compelling result strongly suggests that the CCFs generated by SAHA effectively promote SASP production via activation of the cGAS–STING signaling cascade.

The EZH2 enzyme, which serves as the core catalytic unit of the Polycomb Repressive Complex 2 (PRC2), is responsible for writing the repressive epigenetic mark of histone H3 lysine 27 trimethylation (H3K27me3) (31). Disruption of this critical epigenetic regulator is strongly associated with the progression and poor outcomes across numerous malignancies (31). Extensive clinical and preclinical evidence further establishes that the aberrant overexpression of EZH2 is tightly correlated with aggressive tumor behavior, resistance to conventional therapy, and poor patient survival (28, 32) Specifically within lung cancer, EZH2 is often expressed at high levels (28), leading to its recognition as a viable therapeutic vulnerability due to its established connection with compromised treatment response (33).

Leveraging our prior research, which established the functional role of EZH2 in both the genesis of CCFs and the resultant SASP secretion in breast cancer (24) and SCLC cell lines (25), we proceeded to assess the therapeutic impact of EZH2 inhibition within the context of NSCLC. Our co-treatment protocol, combining SAHA with the EZH2 inhibitor EPZ-6438, led to a highly significant attenuation of IL-6 cytokine levels when compared to the SAHA-only condition. Furthermore, despite this successful suppression of the SASP factor, a subsequent examination of central cGAS–STING pathway components did not reveal any clear change in the phosphorylation status of STING (data not shown). Our results suggest that EZH2 blockade successfully mitigates the SAHA-triggered SASP secretion in NSCLC cells. Nevertheless, the precise molecular pathway responsible for this inhibitory effect has yet to be fully elucidated and necessitates future research. Significantly, the combined therapeutic approach—using both SAHA and the EZH2 inhibitor—preserved the state of cellular senescence. This was evidenced by the lack of meaningful change in the expression of key senescence markers, Cyclin A2 and p21, when compared against the SAHA monotherapy group.

In conclusion, our findings demonstrate that utilizing the HDAC inhibitor SAHA in NSCLC cell lines (A549 and H1299) results in a therapeutic trade-off: successful induction of cellular senescence is inadvertently accompanied by the activation of the detrimental SASP, which is mechanistically driven by SAHA-triggered CCF formation. Crucially, we show that the inhibitory action of the EZH2 inhibitor successfully uncouples these two effects, suppressing the pro-tumorigenic SASP and thereby significantly strengthening SAHA's anti-proliferative capabilities against NSCLC cells. Consequently, we propose that the strategic co-administration of SAHA and an EZH2 inhibitor constitutes a highly promising therapeutic avenue for NSCLC, aiming to curb cancer progression and mitigate recurrence by simultaneously inducing growth arrest and neutralizing the counterproductive SASP.

5. Conclusion

In summary, our study demonstrates that HDAC inhibition by SAHA in NSCLC cells induces a dual effect: it triggers desired cellular senescence but also promotes the detrimental SASP via CCF formation and cGAS-STING pathway activation. Crucially, we found that simultaneously inhibiting EZH2 with EPZ-6438 effectively uncouples these processes. This combination strategy suppresses the pro-tumorigenic SASP while preserving the anti-proliferative state of senescence, thereby leading to a more robust suppression of cancer cell growth.

Acknowledgments

Authors would like to express their gratitude to University of Sciences (PyongYang, DPR Korea) for supporting this study. Artificial intelligence-based technologies have not been used in the production of this work.

Ethical Considerations and Compliance with Ethical Guidelines

There were no ethical considerations to be considered in this research.

Funding

This work was supported by the National Natural Science Foundation of Korea (Grant No. 54289562).

Conflict of interest

The authors declare no conflict of interest, financial or otherwise.Consent to participate.

AI Using Declaration

The authors declare no artificial intelligent chatbot use.

Author's contributions

SHK, HSK, and CJP conceived and designed the study. CJP, SHK, HSK, BSR, JCJ, KCR, and KCK performed the experiments and analyzed the results. SHK, HSK, USR, GMH, CHJ and YMR performed computational analysis. SHK, HSK, CJP and USR drafted and wrote the paper. CJP and GMH supervised the study. All authors agreed to the final version of the manuscript.

6. References

1. Siegel RL, Miller KD, Fuchs HE, Jemal A. Cancer Statistics, 2021. CA: A Cancer Journal for Clinicians. 2021 Jan;71(1):7–33. (DOI: 10.3322/caac.21654) (PMID)

2. Duruisseaux M, Esteller M. Lung cancer epigenetics: From knowledge to applications. Semin Cancer Biol. 2018 Aug;51:11628. (DOI: 10.1016/j.semcancer.2017.09.005) (PMID)

3. Pao W, Miller VA, Politi KA, Riely GJ, Somwar R, Zakowski MF, et al. Acquired resistance of lung adenocarcinomas to gefitinib or erlotinib is associated with a second mutation in the EGFR kinase domain. PLoS Medicine. 2005 Mar; 2(3):e73. (DOI: 10.1371/journal.pmed.0020073) (PMID)

4. Wang B, Kohli J, Demaria M. Senescent Cells in Cancer Therapy: Friends or Foes? Trends in Cancer. 2020 Oct;6(10):838-57. (DOI: 10.1016/j.trecan.2020.05.004) (PMID)

5. Demaria M, O'Leary MN, Chang J, Shao L, Liu S, Alimirah F, et al. Cellular senescence promotes adverse effects of chemotherapy and cancer relapse. Cancer Discovery. 2017 Feb;7(2):165-76. (DOI: 10.1158/2159-8290.CD-16-0241) (PMID)

6. Lecot P, Alimirah F, Desprez PY, Campisi J, Wiley C. Context-dependent effects of cellular senescence in cancer development. British Journal of Cancer. 2016 May;114(11):1180-4. (DOI: 10.1038/bjc.2016.115) (PMID)

7. Gorgoulis V, Adams PD, Alimonti A, Bennett DC, Bischof O, Bishop C, et al. Cellular senescence: defining a path forward. Cell. 2019 Oct;179(4):813-27. (DOI: 10.1016/j.cell.2019.10.005) (PMID)

8. Coppe JP, Desprez PY, Krtolica A, Campisi J. The senescence-associated secretory phenotype: the dark side of tumor suppression. Annual Review of Pathology. 2010;5:99-118. (DOI: 10.1146/annurev-pathol-121808-102144) (PMID)

9. Lederle W, Depner S, Schnur S, Obermueller E, Catone N, Just A, et al. IL-6 promotes malignant growth of skin SCCs by regulating a network of autocrine and paracrine cytokines. International Journal of Cancer. 2011 Jun;128:2803-14. (DOI: 10.1002/ijc.25621) (PMID)

10. Hartman ZC, Poage GM, den Hollander P, Tsimelzon A, Hill J, Panupinthu N, et al. Growth of triple-negative breast cancer cells relies upon coordinate autocrine expression of the proinflammatory cytokines IL-6 and IL-8. Cancer Research. 2013 Jun;73:3470-3480. (DOI: 10.1002/ijc.25621) (PMID)

11. Rojas A, Liu G, Coleman I, Nelson PS, Zhang M, Dash R, et al. IL-6 promotes prostate tumorigenesis and progression through autocrine cross-activation of IGF-IR. Oncogene. 2011 May;30:2345-55. (DOI: 10.1038/onc.2010.605) (PMID)

12. Song L, Rawal B, Nemeth J A, et al. JAK1 activates STAT3 activity in non-small-cell lung cancer cells and IL-6 neutralizing antibodies can suppress JAK1-STAT3 signaling. Molecular Cancer Therapeutics. 2011 Mar;10(3):481-94. (DOI: 10.1158/1535-7163.MCT-10-0502) (PMID)

13. Oubaha M, Miloudi K, Dejda A, Guber V, Mawambo G, Germain MA, et al. Senescence-associated secretory phenotype contributes to pathological angiogenesis in retinopathy. Science Translational Medicine. 2016 Oct;8(362):362ra144. (DOI: 10.1126/scitranslmed.aaf9440) (PMID)

14. Ivanov A, Pawlikowski J, Manoharan I, van Tuyn J, Nelson DM, Rai TS, et al. Lysosome-mediated processing of chromatin in senescence. Journal of Cell Biology. 2013 Jul;202(1):129-43. (DOI: 10.1083/jcb.201212110) (PMID)

15. Dou Z, Ghosh K, Vizioli MG, Zhu J, Sen P, Wangensteen KJ, et al. Cytoplasmic chromatin triggers inflammation in senescence and cancer. Nature. 2017 Oct;550(7676):402-6. (DOI: 10.1038/nature24050) (PMID)

16. Yang H, Wang H, Ren J, Chen Q, Chen ZJ. cGAS is

essential for cellular senescence. Proceedings of the National Academy of Sciences of USA. 2017 Jun;114(23):E4612-E20. (DOI: 10.1073/pnas.1705499114) (PMID)

17. Glück S, Guey B, Gulen MF, Wolter K, Kang TW, Schmacke NA, et al. Innate immune sensing of cytosolic chromatin fragments through cGAS promotes senescence. Nature Cell Biology. 2017 Sep;19(9):1061-70. (DOI: 10.1038/ncb3586) (PMID)

18. Krupina K, Goginashvili A, Cleveland DW. Causes and consequences of micronuclei. Current Opinion in Cell Biology. 2021 Jun;70:91-9. (DOI: 10.1016/j.ceb.2021.01.004) (PMID)

19. Fardi M, Solali S, Farshdousti Hagh M. Epigenetic mechanisms as a new approach in cancer treatment: An updated review. Genes & Diseases. 2018 Jun;5(4):304-11. (DOI: 10.1016/j.gendis.2018.06.003) (PMID)

20. Zhu P, Martin E, Mengwasser J, Schlag P, Janssen KP, Göttlicher M. Induction of HDAC2 expression upon loss of APC in colorectal tumorigenesis. Cancer Cell. 2004 May;5(5):455-63. (DOI: 10.1016/s1535-6108(04)00114-x) (PMID)

21. Ropero S, Fraga M F, Ballestar E, et al. A truncating mutation of HDAC2 in human cancers confers resistance to histone deacetylase inhibition. Nature Genetics. 2006 May;38(5):566-9. (DOI: 10.1038/ng1773) (PMID)

22. Li Z, Zhu W G. Targeting histone deacetylases for cancer therapy: from molecular mechanisms to clinical implications. International Journal of Biological Sciences. 2014 Jul;10(7):757-70. (DOI: 10.7150/ijbs.9067) (PMID)

23. Almeida LO, Guimarães DM, Martins MD, Martins MAT, Warner KA, Nör JE, et al. Unlocking the chromatin of adenoid cystic carcinomas using HDAC inhibitors sensitize cancer stem cells to cisplatin and induces tumor senescence. Stem Cell Research. 2017 May;21:94-105. (DOI: 10.1016/j.scr.2017.04.003) (PMID)

24. Duan D, Shang M, Han Y, Liu J, Liu J, Kong SH, Hou J, et al. EZH2–CCF–cGAS Axis Promotes Breast Cancer Metastasis. International Journal of Molecular Sciences. 2022 Feb;23(3):1788. (DOI: 10.3390/ijms23031788) (PMID)

25. Kong SH, Ma L, Yuan Q, Liu X, Han Y, Xiang W, et al. Inhibition of EZH2 alleviates SAHA-induced senescenceassociated secretion phenotype in small cell lung cancer cells. Cell Death Discovery. 2023 Aug;9(1):289. (DOI: 10.1038/s41420-023-01591-y) (PMID)

26. Hernandez-Segura A, Nehme J, Demaria M. Hallmarks of Cellular Senescence. Trends in Cell Biology. 2018 Jun;28(6):436-53. (DOI: 10.1016/j.tcb.2018.02.001) (PMID)

27. Kumari R, Jat P. Mechanisms of Cellular Senescence: Cell Cycle Arrest and Senescence Associated Secretory Phenotype. Frontiers in Cell and Developmental Biology. 2021 Mar;9:645593. (DOI: 10.3389/fcell.2021.645593) (PMID)

28. Behrens C, Solis LM, Lin H, Yuan P, Tang X, Kadara H, et al. EZH2 protein expression associates with the early pathogenesis, tumor progression, and prognosis of non-small cell lung carcinoma. Clinical Cancer Research. 2013 Dec;19:6556–65. (DOI: 10.1158/1078-0432.CCR-12-3946) (PMID)

29. Ewald JA, Desotelle JA, Wilding G, Jarrard DF. Therapy-induced senescence in cancer. Journal of the National Cancer Institute. 2010 Oct;102(20):1536-46. (DOI: 10.1093/jnci/djq364) (PMID)

30. Prantner D, Perkins DJ, Lai W, Williams MS, Sharma S, Fitzgerald KA, et al. 5,6-Dimethylxanthenone-4-acetic acid (DMXAA) activates stimulator of interferon gene (STING)-dependent innate immune pathways and is regulated by mitochondrial membrane potential. Journal of Biological Chemistry. 2012 Nov;287(47):39776-88. (DOI: 10.1074/jbc.M112.382986) (PMID)

31. Sparmann A, van Lohuizen M. Polycomb silencers control cell fate, development and cancer. Nature Reviews Cancer. 2006 Nov;6(11):846–56. (DOI: 10.1038/nrc1991) (PMID)

32. Zhang JX, Chen LY, Han L, Shi ZD, Zhang JN, Pu PY, et al. EZH2 is a negative prognostic factor and exhibits pro-oncogenic activity in glioblastoma. Cancer Letters. 2015 Jan;356(2 Pt B):929-36. (DOI: 10.1016/j.canlet.2014.11.003) (PMID)

33. Kim KH, Roberts CW. Targeting EZH2 in cancer. Natature Medicine. 2016 Feb;22(2):128-34. (DOI: 10.1038/nm.4036) (PMID)